Cyclic Behavior of Dual-Steel Beam-to-Column Welded Flange-Bolted Web Connections

Fangxin Hu[a,b,*], Zhan Wang[a,b]

[a]*School of Civil Engineering and Transportation, South China University of Technology, Guangzhou, 510640, China*
[b]*State Key Laboratory of Subtropical Building Science, South China University of Technology, Guangzhou, 510640, China*

Abstract

Cyclic loading tests on dual-steel beam-to-column welded flange-bolted web connections were conducted to quantify their moment resistance, plastic deformation and energy dissipation capacities. The test program consisted of five one-sided connection specimens, where Q355 grade beams and Q690 grade columns were used, to study the effects of beam-to-column welded flange connection details and panel zone shear strength on the connection seismic performance. Two types of welded connection details were considered, one was the traditional complete-joint-penetration (CJP) welded connections by use of backing bars, and the other type was those with the bottom backing bar further reinforced by a fillet weld. Three column web thicknesses were designed to arrive at strong, intermediate and weak panel zones, respectively. It was found that the CJP weld with the backing bar reinforced only under the bottom beam flange produced satisfactory performance and accommodated plastic rotations larger than 0.03 rad, while a maximum plastic rotation of 0.04 rad could be developed in the high-strength steel panel zone before fracture occurred. These results evidenced that those dual-steel connections could still sustain high seismic deformation demands.

Keywords: Joint, High-strength steel, Dual-steel, Joint, Welded flange-bolted web connection, Cyclic, Experiment

*Corresponding author
Email address: hufx@scut.edu.cn (Fangxin Hu)

1 Introduction

High-strength steels with yield strength of at least 460MPa have become an economical alternative to conventional-strength steels, since the former steels enable increased cross-sectional strength, and thus smaller cross sections to be used for the same loading condition [1–6]. This performance allows for more economical and ecological construction. High-strength steels have distinct material properties from the conventional ones. In addition to the increased yield and ultimate tensile strength, decreased ductility is expected in high-strength steels [7–9]. This matters if the plastic deformation capacity is concerned, such as in plastic design and seismic design.

For typical steel moment-resisting frames, ductile performance of beam-to-column connections is critical to assure structural safety under severe earthquakes. Several studies have been conducted on the seismic behavior of high-strength steel beam-to-column connections. The first study maybe dates back to the 1990s, when Kuwamura and Suzuki [10] investigated the low-cycle fatigue resistance of beam-to-column fully welded joints of a new, though at that time, type of heat-treated 600MPa tensile-strength grade high-strength steel with yield ratios not more than 80%. They found that the joints had an enough safety margin against a strong earthquake motion of the ultimate intensity prescribed in then Japanese seismic design code, in terms of average and cumulative ductilities. Dubina et al. [11] carried out an extensive testing program to evaluate the monotonic and cyclic performance of moment-resisting joints of high-strength steel and mild carbon steel components, including fully welded connections between S235 beams and S355/S460 columns. Stiffeners were used to strengthen the connection zone near the flange welds. Therefore, the connections developed substantial ultimate rotations of nearly 0.1 rad and 0.06–0.08 rad under monotonic and cyclic loadings, respectively, before final fracture at the stiffener in tension. Those rotations were almost all contributed by panel zones in the connections. Oh and Park [12] studied the deformation capacity of beam-to-column fully welded connections using HSA800 grade steel with a target tensile strength of 800 MPa (yield strength of 650–770 MPa, and a yield-to-tensile ratio of 0.85 or less) under cyclic loading. It was found that the traditional welded-type connection with weld access holes and backing plates for groove welds at the end of beam flanges sustained limited plastic rotation (less than 0.01 rad), while the alternative without weld access holes and backing plates, yet reinforced by a fillet weld at the root of each groove weld, survived a plastic rotation of more than 0.01 rad. They also studied the reinforced connections they proposed using horizontal stiffeners of different shapes to widen the beam flange at the connections, which developed plastic rotations of 0.03 rad or higher. Liao et al. [13] studied the seismic performance of Q460 high-strength steel fully welded cruciform beam-to-column connections, and the effects of weld access holes and locally widened beam flange at the connection. They reported that the connections exhibited ultimate displacements of 80–90 mm (corresponding to story drift angles of 0.053–0.06rad), demonstrating good deformation capacity, although the eventual failure all belonged to cracking and fracture at the beam flange for the unreinforced connections, and cracking between the panel zone and the column flange for the only reinforced connection. Kim et al. [14] investigated experimentally the cyclic behavior of fully welded and extended end-plate beam-to-column connections made of SHN490 and SM490 high-strength steels (measured yield strength of about 450 MPa or above). For the fully welded connections, very large rotations (0.05 rad and 0.06 rad for SHN490 and SM490 specimens, respectively) were recorded even at the maximum moment resistance, before the severe shear instability of the panel zone and the final complete fracture of the flange. Wang et al. [15] conducted an experiment on the fully welded connection between a Q355 grade beam and a Q460 grade column, and this connection specimen developed a maximum story drift angle of over 0.035 rad but it was not tested to failure in the end. Liu et al. [16] investigated the low-cycle fatigue fracture behavior of welded flange-bolted web beam-to-column connections made of Q460C high-strength steel and compared the performance among different welding details and weld access holes. They found that the connections developed plastic rotations of

0.02–0.03 rad before the fracture at the beam flange. Lu [17] examined the cyclic behavior of welded flange-bolted web connections made of Q460GJ, Q550GJ and Q690GJ high-strength steels, as part of a series of experimental tests on high-strength steel connections of various types. However, very limited plastic rotations (less than 0.01 rad) were achieved for these connections.

In addition to the above unreinforced connections, some studies have also been conducted on cover-plate and flange-plate reinforced connections using high-strength steels in China [17–23], and these studies evidenced satisfactory performance of these connections in terms of ultimate rotation capacity, which was basically above 0.04 rad. Besides, Girão Coelho et al. [24] evidenced by a series of experiments that S690 and S960 steel web shear panels were able to undergo shear distortions in the range of 0.05 rad to over 0.1 rad, depending on the panel slenderness, aspect ratio and axial load level. This research qualified those high-strength steel shear panels as a high-ductile connection component. This superior inelastic shear deformation capacity (above 0.1 rad) was also confirmed by Jordão et al. [25, 26], although their attention was mainly drawn to the assessment of the plastic resistance of column web panels subjected to shear and load introduction (compression and tension). Luo et al. [27] showed by an experimental study that the H-shape beam-to-column joint panels made up of H-SA700B high-strength steel were able to develop plastic distortions of 0.025–0.035 rad under cyclic loading before the final weld fracture between the beam and column flanges. The real deformation capacity of this type joint panel should be more than 0.035 rad, since the panels alone were not tested to failure.

Those previous studies clearly shed some light on the inelastic deformation capacity of high-strength steel beam-to-column connections under monotonic and cyclic loadings. But the rotation information on individual high-strength steel connection components, such as the plastic hinge formed at the beam end, and the shear panel, is still very limited, especially for seismic consideration. High-strength steels are expected to be applied in columns with a higher priority than in beams, as strong column-weak beam (SCWB) is to be assured in seismic design. In this way, dual-steel beam-to-column connections, where the beam and column are made up of conventional-strength and high-strength steels, respectively, should be a promising connection type in seismic resistant steel building frames, as pointed out by Dubina et al. [28]. As mentioned above, the available research concerning this type dual-steel connections is limited to 460 MPa yield-strength grade steel and fully welded type [11, 15], and most of the relevant studies did not succeed to evaluate the real cyclic deformation capacity of joint components, in particular, of high-strength steel shear panels. More research on dual-steel beam-to-column welded flange-bolted web connections, which may be the most widely used connection type in steel construction due to its convenient fabrication and erection, is in urgent need.

Therefore, cyclic tests on typical dual-steel welded unreinforced flange-bolted web (WUF-B) connections, where Q355 grade beams and Q690 grade columns were used, were carried out in this paper to evaluate their moment strength, deformation and energy dissipation capacities. The cyclic test program is presented, followed by test results. Discussions are then presented regarding the validity of present seismic provisions for this connection design. The goal of this study is to obtain real plastic rotation capacity and develop seismic design recommendations on this type connections.

2 Test program

2.1 Design of specimens

The T-shape assembly which represents an exterior beam-to-column joint in a moment frame structure was selected for investigation in this paper. As shown in Figure 1, the beam and column sizes of the subassemblage were determined by a proper design of the prototype three-bay six-story plane moment frame. The dead (D) and live (L) loads are 6 kN/m^2 and 2 kN/m^2, respectively. The story height (H) is 3000 mm, and the in-plane and out-of-plane column spacings (L) are both 6000 mm. When subjected to lateral loads such as earthquakes, such a prototype frame is expected to exhibit reverse curvature bending both in its columns and beams, with inflection points occurring near the mid-span of the beams and mid-height of the columns. This assumption is reasonable when the gravity load is small in comparison to the seismic load. In the T-shape specimen, the column inflection points are simulated with load pins at both the top and bottom of the column, while the free end of the beam at the point of actuator attachment simulates the beam inflection point, as described in the following section.

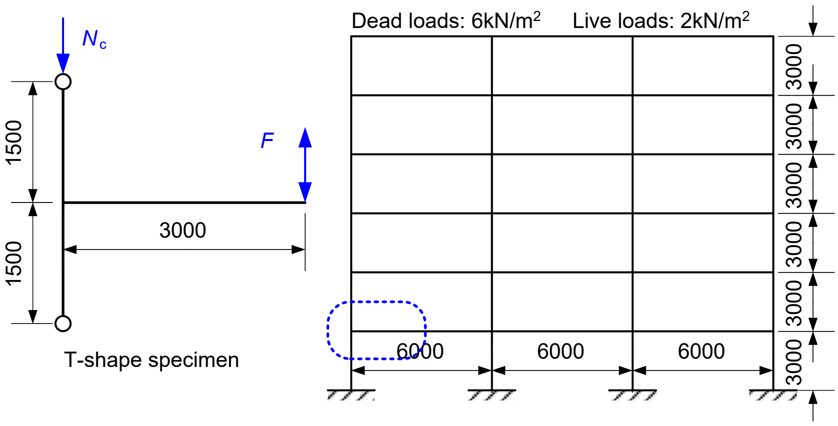

Figure 1. Extraction of the T-shaped assembly (unit: mm)

Beams and columns in the prototype frame were made of Q355 (conventional-strength) and Q690 (high-strength) grade steels, respectively. They were checked for both the ultimate and serviceability limit states. As for the former limit state, a factored non-seismic (or say, fundamental) load combination, 1.3D + 1.5L, was taken into account to check the beam strength, column strength and stability. Strength and stability were also satisfied under another factored seismic load combination, $1.2\,(\mathrm{D} + 0.5\mathrm{L}) + 1.3\mathrm{E}_{\mathrm{hk1}}$, where $\mathrm{E}_{\mathrm{hk1}}$ represents the design seismic action of the frequently-occurred 1st-group earthquake in a intensity-8 region of ground type II, according to Chinese Seismic Code [29]. Generally, it is required that the beams in earthquake-resistant frames be braced adequately to avoid lateral-torsional buckling, and thus the instability of beams was not considered. To cater for the latter limit state, the maximum beam deflection was within the code rated limit, 1/400 of the beam span, under a nominal (or say, characteristic) non-seismic load combination, D + L. Besides, the maximum story drift angle under the above-mentioned frequently-occurred earthquake was required not to exceed 1/250. As a result, a built-up H-shaped section, H320×160×8×14, was used for the Q355 steel beams. However, for the Q690 steel columns, three built-up H-shaped sections, i.e, H240×160×8×12, H240×160×10×12 and H240×160×12×12 that are different only in the web thickness but all satisfying the strong column-weak beam (SCWB) capacity design, were designed to facilitate the evaluation of the impact of panel zone strength.

Five specimens were designed as summarized in Table 1. Each connection specimen had complete joint penetration (CJP) welds connecting the beam flanges to the column flange, and an erection plate (or shear tab) of the same steel grade and thickness to the beam web, shop-welded to the column flange with fillet welds and bolted to the beam web for transfer of shear force. Three web connection bolts used in each specimen were all class 10.9s M20 high-strength bolts with pretension force of 155kN [30]. Continuity plates as required, were also used in this study with the same steel grade, width and thickness to the corresponding beam flanges, to prevent local damage to the column flange and web and to help assure uniform stress in the beam flanges. In addition to the varying column web thickness, two types of CJP welded connection details between the beam and column flanges as shown in Figure 2 were included in this investigation for comparison. The type *a* detail with arc-shaped weld access holes, as shown in Figure 2(a), is representative of the typical practice that has been commonly used before the Northridge earthquake in the United States due to its simplicity [31], but many connections of this type suffered from weld brittle fracture, especially at the bottom flange of the beam. Therefore, the type *b* detail has been developed where a reinforcing fillet weld is placed under the bottom backing bar while the top backing bar is not reinforced [31], and the access hole holes are machined with improved shape specified in AISC Prequalified Connections [32] to alleviate stress concentrations in the transition region between the beam flange and the drilled hole, as shown in Figure 2(b). This type *b* detail is currently recommended in Chinese Seismic Code [29] and Technical Specification [33]. As such, the specimen labels shown in Table 1 begin with the beam and column steel grades, followed by the panel zone thickness, and end with *a* or *b* indicating the beam-to-column flange welded connection detail.

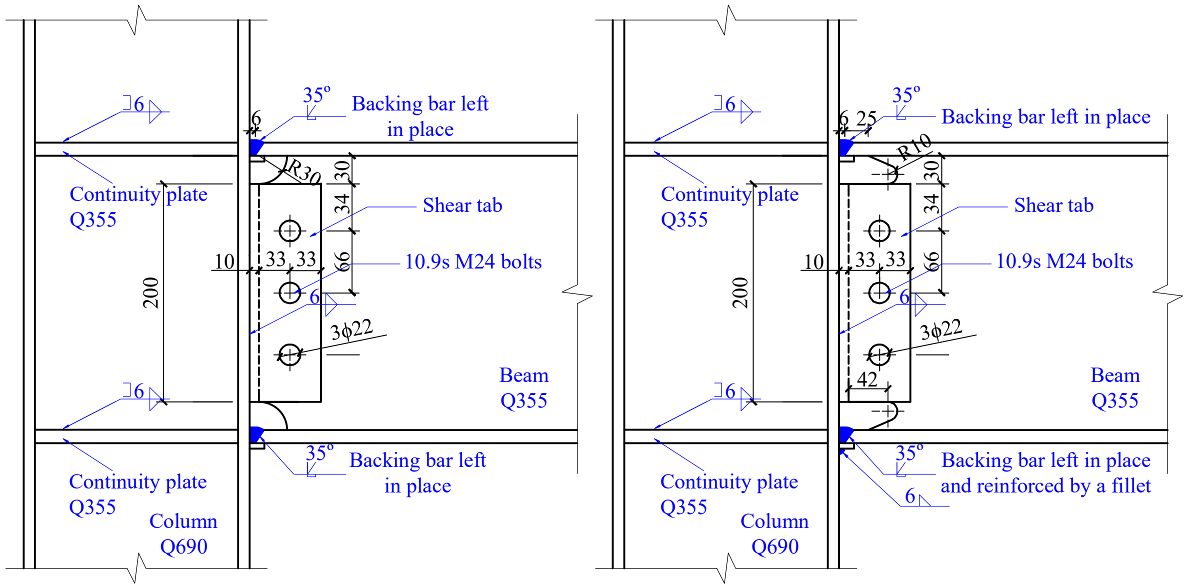

(a) Type *a* (b) Type *b*

Figure 2. Connection details

Table 1. Test specimens

Specimen label	Beam		Column		Welding type
	Steel grade	Cross-section size (mm)	Steel grade	Cross-section size (mm)	
B355-C690-PZ12*a*	Q355	H320×160×8×14	Q690	H240×160×12×12	*a*
B355-C690-PZ12*b*					*b*
B355-C690-PZ10*a*				H240×160×10×12	*a*
B355-C690-PZ10*b*					*b*
B355-C690-PZ8*b*				H240×160×8×12	*b*

Manual gas shielding arc welding with matching weld materials was used in this study. An E761T1-K3C electrode, which fits to Q690 steel grade as stipulated in newly published Chinese Design Standard for High-Strength Steel Structures [34] was used for the fillet welds in producing the welded H-sections for the Q690 columns. The other weldments, including the CJP welds between the beam and column flanges, were implemented using E49 type electrodes that fit to Q355 steel [35].

2.2 Material properties

Material testing was performed on all the steel plates used for the test specimens. Tensile coupon tests were conducted to characterize stress–strain responses of the steel plates. Results of the coupon tests were compared to the requirements for high-strength steel plates in the corresponding codes, so as to ensure those steel plates in this study were qualified. Three coupons were tested for each plate thickness. Full-thickness coupons were used, with a gauge length and width of 50mm and 20mm, respectively. Several quantities were obtained for each plate thickness, including the modulus of elasticity (E), the yield strength (f_y) on the yield plateau or at a 0.2% offset strain when the plateau is absent, the strain at the end of the yield plateau (or at the onset of the strain hardening branch of the stress–strain curve, ϵ_{st}) if any, the ultimate strength (f_u) and its corresponding ultimate strain (ϵ_u), yield-to-tensile strength ratio (f_y/f_u) and percent elongation after fracture based on the specified parallel length (δ) [36], as summarized in Table 2, where each value represents the average of three coupons. As a example, the engineering stress–strain curves of Q690 grade steel coupons are shown in Figure 3. Simple tensile testing on the class 10.9s M20 high-strength bolts used in this study was also undertaken to obtain the modulus of elasticity (E), the ultimate strength (f_u) and ultimate strain (ϵ_u), as also shown in Table 2.

Table 2. Material properties

Steel grade	Plate thickness (mm)	E (GPa)	f_y (MPa)	ϵ_{st}	f_u (MPa)	ϵ_u	f_y/f_u	δ
Q355	8	205.0	406	0.014	539	0.153	0.75	25%
	14	203.5	368	0.020	522	0.200	0.70	29%
Q690	8	208.3	723	—	822	0.100	0.88	20%
	10	189.4	794	—	902	0.106	0.88	21%
	12	205.8	775	0.018	816	0.060	0.95	16%
	16	219.8	811	0.022	840	0.055	0.97	17%
10.9s	M20	206.0	—	—	1135	0.110	—	—

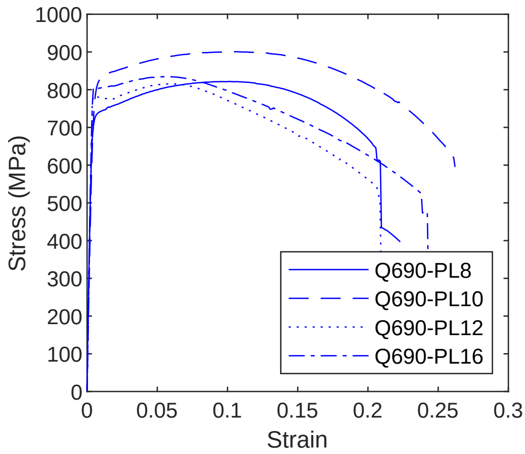

Figure 3. Stress–strain curves of Q690 coupons

2.3 Test setup

A load frame assembly was used for testing conducted in the Structures Laboratory of South China University of Technology. It consists of a system of members designed to form a planar frame to transfer the forces from a jack and another actuator, which are installed within the load frame, to the strong floor of the laboratory. Figure 4 shows the features of the load frame. The T-shape specimen was placed within the load frame and was attached at the top and bottom of the column to large load pins, which in turn, were connected to the crosshead of the 300 t jack at the top and to the large beam at the bottom of the load frame tied to the strong floor. In this way, free rotation of the column ends during loading was allowed, simulating inflection points at the mid-height of the columns of each story. The pins were fabricated from thick plate material and solid steel dowels. Loading was applied on the top of column by the jack and then to the beam tip by the MTS hydraulic actuator, which is capable of 300 kN at a stroke of ±250 mm. The actuator was attached to the beam by a pair of end plates jointed with high-strength threaded steel rods. The top of the actuator was attached tightly to the top beam of the load frame.

Out-of-plane movement of the beam due to lateral-torsional buckling was restricted by a pair of brackets attached to an additional pair of columns tied down to the strong floor. The brackets were designed with rollers so that the effects of potential friction between the brackets and the

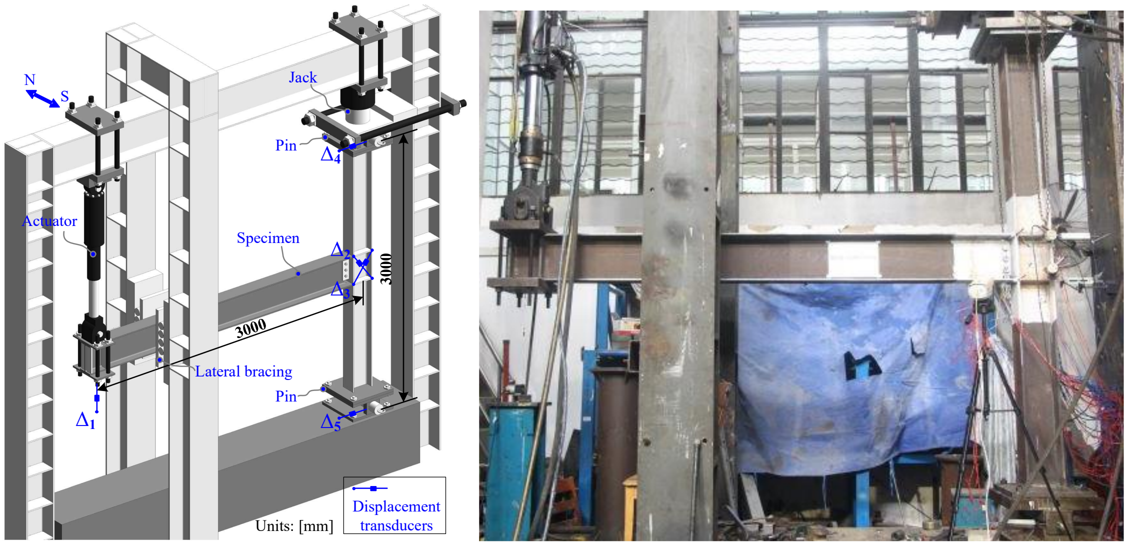

(a) Scheme (b) On site

Figure 4. Test setup

beam were negligible.

2.4 Loading protocol

Before the start of cyclic loading, a constant axial compression force was imposed on the top of the column to represent seismic weight. This introduced an axial compression ratio of 0.3 with respect to the nominal axial capacity of the column, which remained the same in all the specimens to ensure consistency. At the cyclic loading stage, while the axial load on the column top remained unchanged, the loading history in AISC Seismic Provisions [37] was used to ensure results could be compared to numerous other tests conducted during and after the SAC Joint Venture investigations in the Unites States [31]. This cyclic loading history at the beam tip is based on the story drift angle instead of plastic rotation levels that may be employed popularly prior to the Northridge earthquake. The story drift angle is defined as the lateral story displacement divided by the story height. However, the specimens were loaded actually by applying displacements to the tip of the beam. Thus, the story drift angle in this study is defined as the ratio of the beam tip displacement to the distance ($L/2$, where L is the column spacing in the prototype frame) between the beam tip loading point and the column centerline, which is 3000 mm. Figure 5 gives the prescribed loading history, where positive story drift angles indicate downward displacements at the beam tip. As the stroke of the actuator is ±250 mm, this indicates that the maximum story drift angle that can be reached is ±8%. If there is no apparent strength degradation observed after two cycles at 8%, additional cycles at this amplitude would be continued until failure of the specimen or further significant strength degradation occurs.

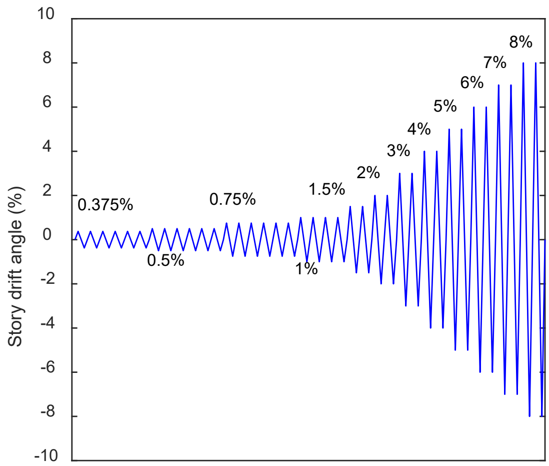

Figure 5. Loading protocol

2.5 Instrumentation

The actuator and the jack were equipped with load cells to measure the magnitude of the applied load at the beam tip and on the column top, respectively. As shown in Figure 4, displacement transducers were used to isolate the inelastic rotations which developed in individual connection components of each specimen, i.e., the shear distortion of the panel zone and the plastic hinge rotation in the beam end. The primary displacement transducer labeled DT-1 measured the displacement at the beam tip. This instrument was used as the displacement-control signal to the actuator. Displacement transducers DT-2 and DT-3 were arranged diagonally to measure the average shear deformation of the panel zone, since shear distortion of the panel zone contributes at a large proportion to the total story drift angle especially for specimens designed with weak panel zone. Another two transducers DT-4 and DT-5 attempted to monitor the horizontal displacements at the center of pins connected to the top and bottom of the column. In this way, taking into account the possible rigid rotation of the entire specimen, the story drift angle, θ, is:

$$\theta = \frac{\Delta_1}{L/2} - \frac{\Delta_4 - \Delta_5}{H} \tag{1}$$

where Δ_1, Δ_4 and Δ_5 are readings from the corresponding labeled displacement transducers, L is the distance (6000 mm) explained above and H is the story height between the pin centerlines (3000 mm). The panel zone shear distortion, γ_{pz}, is:

$$\gamma_{\mathrm{pz}} = \frac{\Delta_2 - \Delta_3}{2} \frac{\sqrt{b_{\mathrm{pz}}^2 + h_{\mathrm{pz}}^2}}{b_{\mathrm{pz}} h_{\mathrm{pz}}} \tag{2}$$

where Δ_2 and Δ_3 are readings from the diagonal transducers, b_{pz} and h_{pz} are the width and height of the panel zone, which are taken as distances between the column flange centerlines and continuity plate centerlines, respectively. The contribution of the panel zone shear distortion to the beam tip displacement, or equivalently, to the story drift angle relative to the column centerline, is given as [38]:

$$\theta_{\mathrm{pz}} = \left(1 - \frac{h_{\mathrm{b}}}{H}\right) \gamma_{\mathrm{pz}} \tag{3}$$

where h_{b} is the beam depth. The rotation contribution of the plastic hinge in the beam end, if developed, could be found by subtracting the contribution of the panel zone from the total story drift angle.

3 Test results

3.1 Failure modes

Depending on the welding type and panel zone strength, the specimens exhibited various failure modes, as summarized in Figure 6. Basically, fracture occurred due to the compact cross sections used in the beams and columns, but the location of fracture differed among them. If the panel zone had intermediate strength or was even strong, the beam flanges near the column face developed cracking and final fracture along the welding fusion face, for example, in Specimens B355-C690-PZ12*a* and B355-C690-PZ10*a*, when the story drift angle reached -1.7% in the second negative excursion to -6%, and -3.5% in the first negative excursion to -5%, respectively (see Figures 6(a) and 6(c)). If the panel zone was weak enough, shear fracture appeared in the column web panel as in Specimen B355-C690-PZ8*b* when the story drift angle reached 6% in the positive excursion of the fourth cycle of 8% (see Figure 6(e)).

It should be borne in mind that the first tested specimen is B355-C690-PZ12*b*, which eventually failed by the weld fracture between the column flange and continuity plates in cycles at the story drift angle of 5% (see Figure 6(b)). Fracture was initially developed in the welds between the top continuity plates and the column flange under positive loading when the story drift angle arrived at 5% for the first time. This fracture was associated with cracking between the column flange and web close to the fractured continuity plate welds. When the loading was continued in the negative direction and the story drift angle reached -5%, the bottom continuity plate welds to the column flange fractured in a similar pattern. After inspection, it was found that the fillet welds were mistakenly used to join the continuity plates and the column flanges, since it is specified in the code that the more expensive CJP groove welds be used instead. This mistakenly used fillet welds had an inadequate thickness of only about 6 mm, which should be responsible for the premature weld fracture. Since the fillet welding rather than the CJP welding had been used in fabrication of all the specimens, it was decided that those continuity

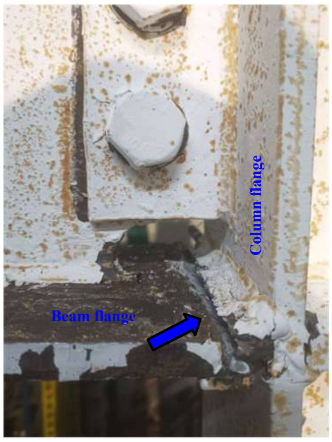

(a) Specimen B355-C690-PZ12*a*

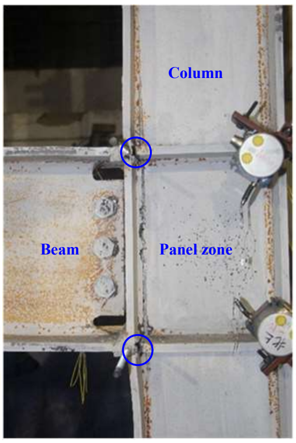

(b) Specimen B355-C690-PZ12*b*

(c) Specimen B355-C690-PZ10*a*

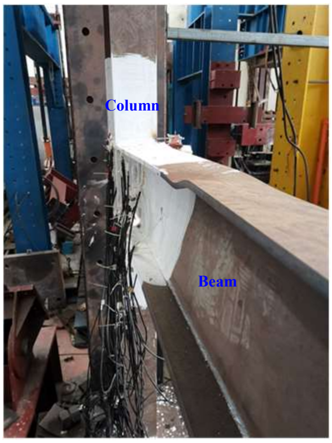

(d) Specimen B355-C690-PZ10*b*

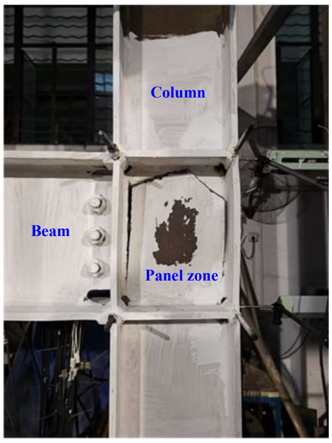

(e) Specimen B355-C690-PZ8*b*

Figure 6. Failure modes

plate-to-column fillet welds in the rest specimens were reinforced to a thickness of 12 mm by overlay welding. Results of the rest specimens evidenced the adequate performance of this type of reinforced fillet welds in seismic conditions.

It should be also explained that Specimen B355-C690-PZ10*b* developed notable lateral-torsional buckling of the beam in cycles of the 7% story drift angle (see Figure 6(d)). This was because the span of lateral bracing was not broad enough to accommodate such a large flexural deformation of the beam at this amplitude.

3.2 Hysteresis curves

Moment–story drift angle hysteresis curves are shown in Figure 7 for all the specimens, where the moment corresponds to the column face and was calculated as the product of the distance between the loading point at the beam tip to the column face, i.e., 3000 mm minus half of the column depth, and the reaction force at the beam tip. The yielding and full plastic moment levels of the beam cross section, $M_{\mathrm{y,b}}$ and $M_{\mathrm{p,b}}$, determined from the measured material properties shown in Table 2, are also plotted for comparison. Besides, the moment–shear distortion hysteresis curves for all the panel zones in those specimens are shown in Figure 8, where the moment is the same to the above, while the shear distortion was calculated using Eq. (2). The yielding moment of the panel zone in an average sense considering the effect of axial compression and column shear, which is indicated in Figure 8 for comparison, is

$$M_{\mathrm{y,pz}} = \sqrt{1 - \left(\frac{N_{\mathrm{c}}}{f_{\mathrm{yc}} A_{\mathrm{c}}}\right)^2} \frac{f_{\mathrm{yc}}}{\sqrt{3}} b_{\mathrm{pz}} h_{\mathrm{pz}} t_{\mathrm{pz}} \frac{L - h_{\mathrm{c}}}{L} \frac{H}{H - h_{\mathrm{pz}}} \tag{4}$$

where N_{c} is the axial compression force on the column, $f_{\mathrm{y,c}}$, h_{c} and A_{c} are the material yield strength, cross-sectional height and area of the column, respectively, t_{pz} is the panel zone thickness. Solid triangular symbols were added in these figures to indicate the instant of fracture.

As expected, the hysteresis curves of both the entire specimens and the panel zones were full before the final failure, and the stiffness and strength remained stable through large inelastic deformations, except for Specimen B355-C690-PZ10*b*. This particular specimen failed by lateral-torsional buckling, resulting in somewhat pinching and unsymmetrical responses in positive and negative loading directions. Deterioration of the hysteresis curves of this specimen was noted caused by the lateral-torsional buckling, when the story drift angle exceeded 6%. All the specimens developed the yielding capacity of the beam, and even its full plastic capacity. But there was high risk for exception when the type *a* connection detail was employed. For example, Specimen B355-C690-PZ10*a* failed to develop the full plastic beam moment when loaded in the

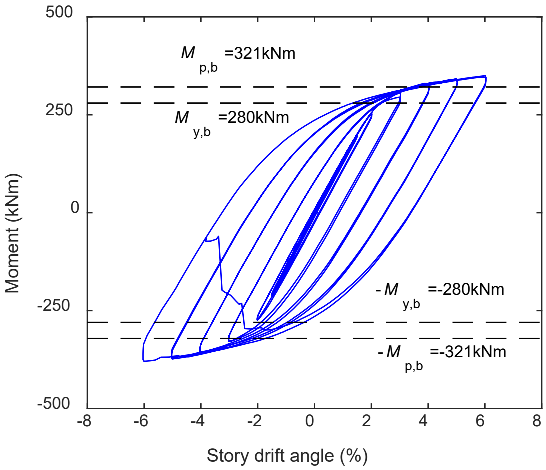

(a) Specimen B355-C690-PZ12*a*

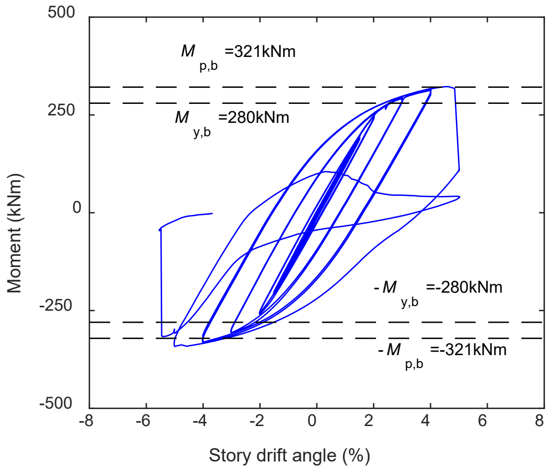

(b) Specimen B355-C690-PZ12*b*

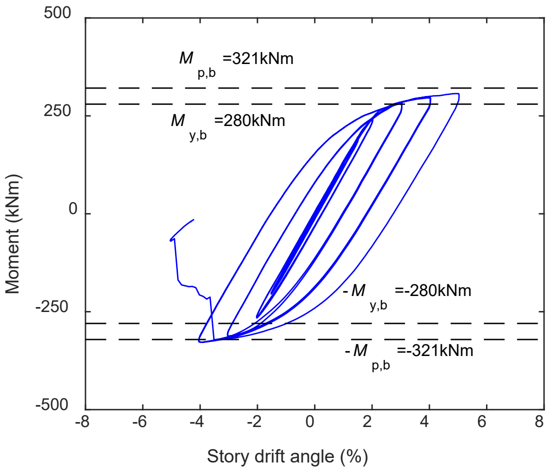

(c) Specimen B355-C690-PZ10*a*

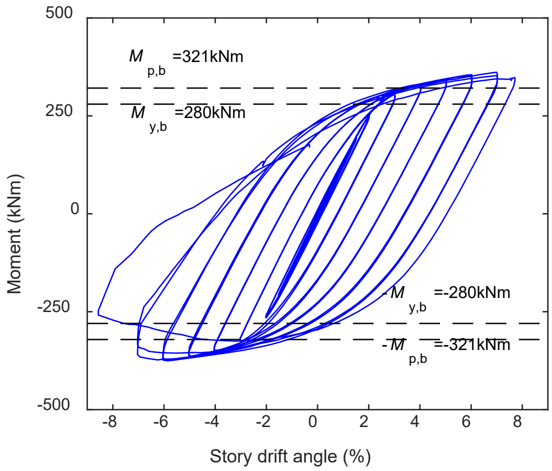

(d) Specimen B355-C690-PZ10*b*

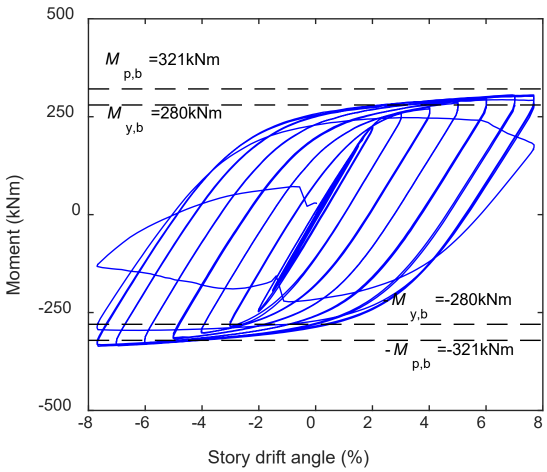

(e) Specimen B355-C690-PZ8*b*

Figure 7. Moment–story drift angle hysteresis curves

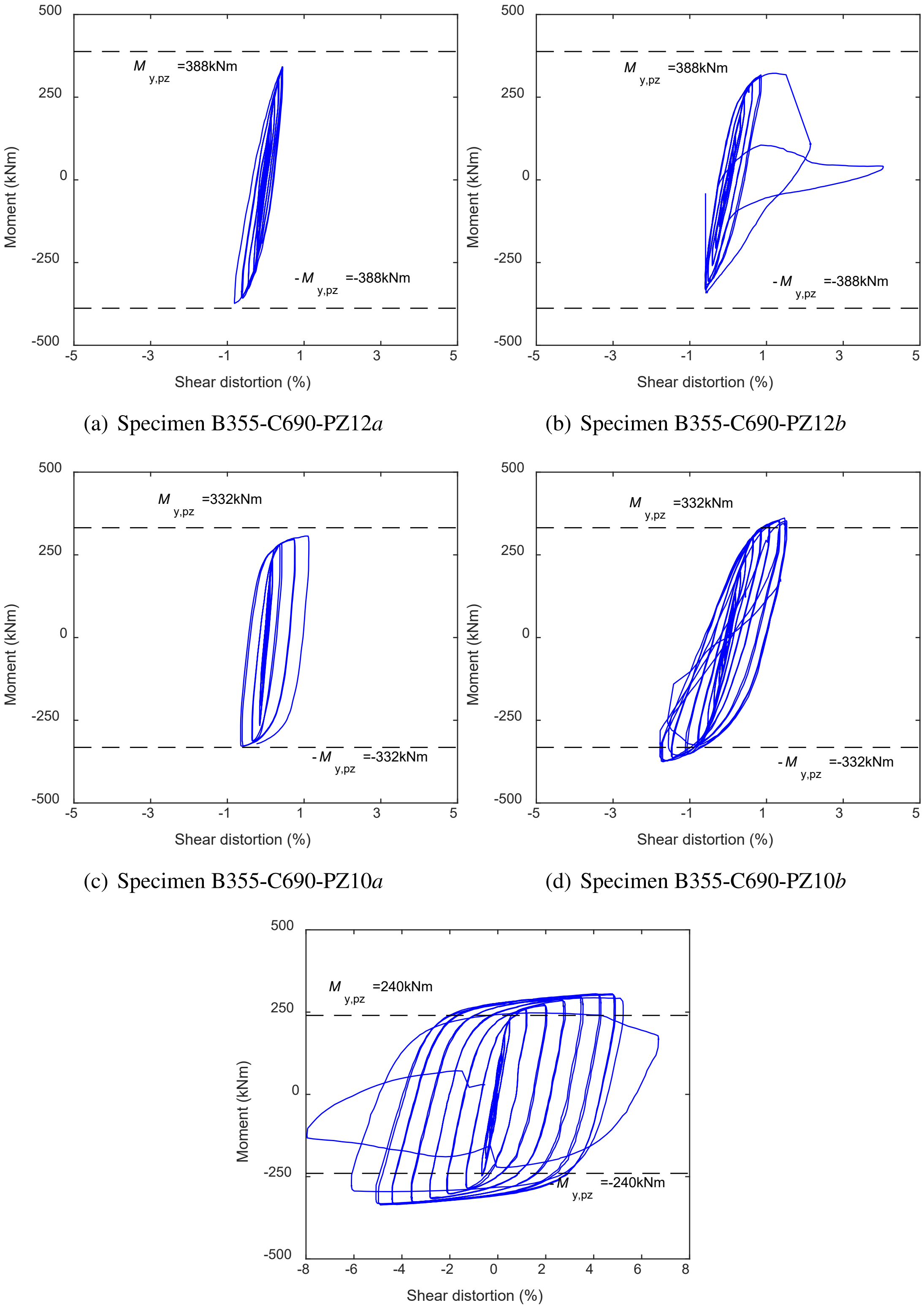

(a) Specimen B355-C690-PZ12*a*

(b) Specimen B355-C690-PZ12*b*

(c) Specimen B355-C690-PZ10*a*

(d) Specimen B355-C690-PZ10*b*

(e) Specimen B355-C690-PZ8*b*

Figure 8. Moment–shear distortion hysteresis curves

positive direction.

As for the panel zone responses, both Specimens B355-C690-PZ12*b* and B355-C690-PZ10*b* exhibited unauthentic results because their failure modes were unexpected. Both should have been avoided by correct seismic design. The panel zone yielding moment in Eq. (4) seemed to lead to overestimation for Specimens B355-C690-PZ10*a* (see Figure 8(c)) and B355-C690-PZ12*a* (see Figure 8(a)), but this might be more likely resulted from the variation in material properties, because a satisfactory agreement was still noted in Specimen B355-C690-PZ8*b* in Figure 8(e). It was interesting to find that even the Q690 high-strength steel panel zone was capable of very large inelastic distortions, as evidenced by this specimen. Considerable plastic hardening was observed in this panel zone, because of the material strain hardening and the participation of the column flanges in shear transfer after the initial yielding of the web panel. This single test confirmed that panel zone yielding resulted in reliable energy dissipation, even in case of high-strength steel used.

3.3 Strength, deformation and energy dissipation

Based on the hysteresis curves in Figure 7, the elastic stiffness, K_e, was determined by linear fit to the data within an amplitude of 1.5% and is shown in Table 3. The ultimate (or maximum) moment, M_u, was identified and is also summarized in Table 3, where $M_\mathrm{p,b}$, $M_\mathrm{y,b}$ and $M_\mathrm{y,pz}$ (see Eq. (4)) are the full plastic and yielding moments of the beam, and the yielding moment of the panel zone, respectively, determined based on the measured material properties. Due to the variation in the measured material strength from the nominal grade values, the specimens with panel zones of thickness of 12mm and 10mm all behaved as connections of strong panel zone design, because their measured $M_\mathrm{y,pz}$ values are even larger than $M_\mathrm{p,b}$ values. On the contrary, Specimen B355-C690-PZ8*b* behaved as expected with a much lower $M_\mathrm{y,pz}$ than $M_\mathrm{y,b}$, and its panel zone did dominate its performance.

Overstrength with respect to $M_\mathrm{y,min}$, the minimum of $M_\mathrm{y,b}$ and $M_\mathrm{y,pz}$, and to the full plastic moment of the beam, $M_\mathrm{p,b}$, denoted as $M_\mathrm{u}/M_\mathrm{y,min}$ and $M_\mathrm{u}/M_\mathrm{p,b}$, respectively, are included in Table 3. The overstrength values show apparent disparity between different connection details. In the

Table 3. Stiffness and strength

<table>
<tr><th>Specimen label</th><th>K_e (kNm)</th><th>$M_{p,b}$ (kNm)</th><th>$M_{y,b}$ (kNm)</th><th>$M_{y,pz}$ (kNm)</th><th>$M_{y,min}$ (kNm)</th><th>M_u (kNm)</th><th>$\frac{M_u}{M_{y,min}}$</th><th>$\frac{M_u}{M_{p,b}}$</th></tr>
<tr><td>B355-C690-PZ12*a*</td><td>13632</td><td rowspan="5">321</td><td rowspan="5">280</td><td rowspan="2">388</td><td rowspan="4">280</td><td>327</td><td>1.17</td><td>1.02</td></tr>
<tr><td>B355-C690-PZ12*b*</td><td>13326</td><td>364</td><td>1.30</td><td>1.13</td></tr>
<tr><td>B355-C690-PZ10*a*</td><td>13271</td><td rowspan="2">332</td><td>318</td><td>1.14</td><td>0.99</td></tr>
<tr><td>B355-C690-PZ10*b*</td><td>13404</td><td>368</td><td>1.32</td><td>1.15</td></tr>
<tr><td>B355-C690-PZ8*b*</td><td>12553</td><td>240</td><td>240</td><td>321</td><td>1.34</td><td>1.00</td></tr>
</table>

specimens with actually strong panel zones (those except for B355-C690-PZ8*b*), the overstrength relative to the yielding moment, $M_u/M_{y,min}$, was about 1.15 when the type *a* connection detail was used, while it was about 1.30 when the type *b* connection detail was used. The overstrength relative to the full plastic moment of the beam, $M_u/M_{p,b}$, also shows the same trend, and was about 1.0 and 1.15 for the connection types *a* and *b*, respectively. This demonstrates the better performance of the type *b* over type *a* in delaying connection failure, so that more strain hardening could be developed. In the specimen with weak panel zone (B355-C690-PZ8*b*), significant strain hardening was developed since its $M_u/M_{y,min}$ reached nearly 1.35, slightly higher than that in the specimens of strong panel zones and the same connection detail (1.30 for B355-C690-PZ12*b* and 1.32 for B355-C690-PZ10*b*). Such high overstrength even led to the full plastic state of the beam ($M_u/M_{p,b}$ of 1.0), which indicates that some inelastic rotation should be expected at the beam end.

Quantities related to deformation and energy dissipation capacities are summarized in Table 4. The yield story drift angle, θ_y, was calculated as $M_{y,min}/K_e$. The ultimate story drift angle, θ_u, was counted only if a least one complete cycle of the target story drift angle was completed before fracture occurred [31]. The plastic story drift angle (or plastic rotation, relative to the column centerline) of the entire connection, θ_p, was identified as the plastic component of θ_u. Table 3 also contains the plastic rotation component in the beam, $\theta_{p,b}$, and that in the panel zone, $\theta_{p,pz}$. The plastic rotation of the panel zone ($\theta_{p,pz}$) was deduced from the total rotation of the panel zone (θ_{pz}) shown in Eq. (3), while the plastic rotation of the beam ($\theta_{p,b}$) was obtained by subtracting $\theta_{\mathrm{p,pz}}$ from θ_{p}. In this way, the ductility factor, μ, was computed as the ratio of θ_{u} to θ_{y}. Cumulative plastic rotations, $\Sigma\Delta\theta_{\mathrm{p}}$, and energy dissipation, ΣA, of the entire specimens were determined based on the method in ATC-24 [39, 40], as shown in Figure 9, and they were counted until the last successful excursion (or half-cycle) before the fracture, as summarized in Table 4 as well as their normalized values by the yielding quantities, $\Sigma\Delta\theta_{\mathrm{p}}/\theta_{\mathrm{y}}$ and $\Sigma A/\left(M_{\mathrm{y,min}}\theta_{\mathrm{y}}\right)$. It should be borne in mind that, Specimen B355-C690-PZ12*b* underwent an unexpected and unreasonable fracture at the continuity plate welds, and so this specimen would not be discussed in the following evaluation. Specimen B355-C690-PZ10*b* experienced also unexpected lateral-torsional buckling, which should have been avoided, and so the results of this specimen could be deemed as conservative.

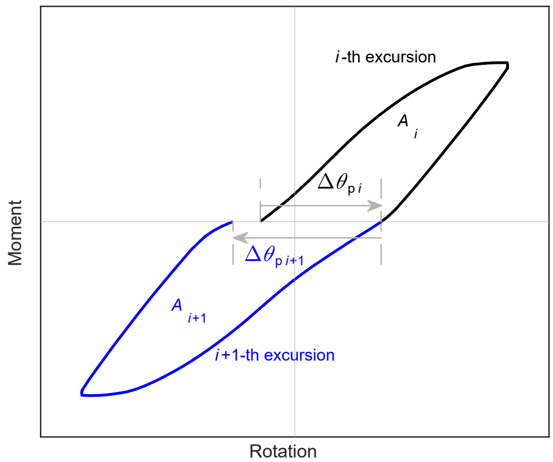

Figure 9. Definition of cumulative plastic rotation and energy dissipation in ATC-24 [39]

Table 4. Deformation and energy dissipation

Specimen label	θ_{y} (rad)	θ_{u} (rad)	μ	θ_{p} (rad)	$\theta_{\mathrm{p,pz}}$ (rad)	$\theta_{\mathrm{p,b}}$ (rad)	$\Sigma\Delta\theta_{\mathrm{p}}$	$\frac{\Sigma\Delta\theta_{\mathrm{p}}}{\theta_{\mathrm{y}}}$	ΣA (kJ)	$\frac{\Sigma A}{M_{\mathrm{y,min}}\theta_{\mathrm{y}}}$
B355-C690-PZ12*a*	0.020	0.06	3.0	0.033	0.003	0.030	0.558	27.1	167.2	27.9
B355-C690-PZ12*b*	0.020	0.04	2.0	0.016	0.003	0.013	0.201	9.5	51.5	8.4
B355-C690-PZ10*a*	0.021	0.04	1.9	0.017	0.005	0.012	0.249	11.8	66.0	10.7
B355-C690-PZ10*b*	0.021	0.07	3.3	0.041	0.004	0.037	1.021	48.9	312.0	51.2
B355-C690-PZ8*b*	0.019	0.08	4.2	0.051	0.039	0.012	1.638	85.7	455.7	95.3

It is clear that, all the specimens developed large story drift angles and very ductile performance was achieved, if a story drift angle of 0.04 rad is deemed sufficient for Special Moment Frames (SMF) in AISC Seismic Provisions [37]. Due to the small sections of the beams and columns used in this study, the yielding drift angles of about 0.02 rad were nearly two times the traditionally expected value (about 0.01 rad). That means, if instead, a plastic rotation of 0.03rad is deemed sufficient, connections using the type *a* connection detail may be judged to have inadequate rotation capacity, such as shown by Specimen B355-C690-PZ10*a*. The other specimens with type *b* connection detail performed well beyond this plastic rotation limit. Moreover, it is shown that the weak panel zone brought further increase in the plastic rotation. This is impressive in that it has been traditionally deemed that excessive deformation in panel zone is detrimental to rotation capacity due to the "kink" formed in column flanges, which results in large local stress or strain concentrations near the flange welds. But this adverse effect was not observed in this study. On the contrary, the panel zone of Q690 grade in the present study sustained as large a plastic shear rotation as about 0.04 rad before its shear fracture, as shown by Specimen B355-Q690-PZ8*b*. This panel zone rotation quantity provides valuable reference in seismic performance evaluation, because none of the previous studies have collected this quantity as real as possible. Besides, the cumulative quantities also demonstrate ductile performance. The cumulative plastic rotations were at least 10 times larger than the amplitude of plastic rotation in case of connection type *a*, were nearly 50 times in case of connection type *b*, and over 80 times if panel zone rotation was dominant. A similar comparison could be made on the cumulative energy dissipation. Those capacities revealed by this study are much higher than the conventional anticipated seismic demand, where the cumulative plastic deformation is five to eight times larger than the maximum plastic deformation [40, 41].

4 Discussions on current seismic provisions

4.1 Welded connection details

In the current Chinese codes relevant to seismic design of steel structures [29, 33, 35], the type *b* connection detail is required for the CJP weld between the beam and column flanges, and the traditional type *a* connection detail is not allowed any more. This requirement was confirmed in the present study because Specimen B355-C690-PZ10*a* with connection type *a* sustained a plastic rotation of less than 0.02 rad, which may be insufficient in ductile structures as mentioned above. In fact, nowadays the welding requirements in the United States are even more strict than the above type *b*. According to AISC Prequalified Connections [32] for Special Moment Frames (SMF) as well as Intermediate Moment Frames (IMF), the fully welded (welded flange-welded web) connection is recommended. The CJP weld with the backing bar reinforced by a fillet is specified at the top beam-to-column flange connection, while the CJP weld without a backing bar (or removed after welding) is specified at the bottom. Therefore, the present study revealed that the welded flange-bolted web connection with the slightly reinforced type *b* connection detail might still be adequate to develop a plastic rotation of not less than 0.03 rad, even when high-strength steel is employed in the column.

As for the continuity plate welds, the present study also shed some light. The above-mentioned Chinese codes and AISC Seismic Provisions generally require CJP groove welds between continuity plates and column flanges, while fillet welds are allowed between continuity plates and the column web. In this study, although the fillet welds were unintentionally used in all the specimens for the connection of continuity plates to column flanges, they performed well throughout the tests, as long as those fillet welds had adequate size. This advantage of using more economical fillet welds than CJP groove welds has been evidenced as well for welded flange-welded web connections made up of conventional-strength steel [42, 43].

4.2 Panel zone

Since the effect of panel zone strength was investigated in this study, it would be necessary to compare the impact of required panel zone strength in different design codes, in order to provide a clear picture of whether the current panel zone design method is adequate or should be revised. Therefore, the present design equations are summarized as follows. In Chinese Standard [35], the moment strength of the panel zone should satisfy

$$\frac{4}{3}\frac{f_{\mathrm{y,pz}}}{\sqrt{3}}h_{\mathrm{pz}}b_{\mathrm{pz}}t_{\mathrm{pz}} \geq \alpha_{\mathrm{pz}}\Sigma W_{\mathrm{p,b}}f_{\mathrm{y,b}} \tag{5}$$

In the United States, it is required by AISC Seismic Provisions [37] that

$$0.6f_{\mathrm{y,pz}}\frac{0.95h_{\mathrm{c}}t_{\mathrm{pz}}h_{\mathrm{b}}}{\beta}\left(1+\frac{3b_{\mathrm{c}}t_{\mathrm{fc}}^2}{h_{\mathrm{b}}h_{\mathrm{c}}t_{\mathrm{pz}}}\right) \geq \min\left(\frac{f_{\mathrm{y,b}}+f_{\mathrm{u,b}}}{2f_{\mathrm{y,b}}}, 1.2\right)\Sigma W_{\mathrm{p,b}}f_{\mathrm{y,b}} \tag{6}$$

It should be mentioned that after the SAC Joint Venture investigations, the panel zone strength is suggested within the lower and upper bounds in the FEMA report [31] as

$$(0.9)\,0.55f_{\mathrm{y,pz}}h_{\mathrm{c}}t_{\mathrm{pz}} \geq \frac{\Sigma W_{\mathrm{y,b}}f_{\mathrm{y,b}}}{h_{\mathrm{b}}}\left(\frac{L}{L-h_{\mathrm{c}}}\right)\left(\frac{H-h_{\mathrm{b}}}{H}\right) \tag{7a}$$

$$(0.6)\,0.55f_{\mathrm{y,pz}}h_{\mathrm{c}}t_{\mathrm{pz}} \leq \frac{\Sigma W_{\mathrm{y,b}}f_{\mathrm{y,b}}}{h_{\mathrm{b}}}\left(\frac{L}{L-h_{\mathrm{c}}}\right)\left(\frac{H-h_{\mathrm{b}}}{H}\right) \tag{7b}$$

Lastly, Eurocode 8 [44] requires that

$$0.9\frac{f_{\mathrm{y,pz}}}{\sqrt{3}}\frac{(h_{\mathrm{c}}-2t_{\mathrm{fc}})\,h_{\mathrm{pz}}t_{\mathrm{pz}}}{\beta}+\frac{2M_{\mathrm{p,fc}}+\min\left(2M_{\mathrm{p,fc}}, 2M_{\mathrm{p,st}}\right)}{\beta} \geq \Sigma W_{\mathrm{p,b}}f_{\mathrm{y,b}} \tag{8}$$

In the above equations, $f_{\mathrm{y,pz}}$ is the material yield strength of the panel zone, $f_{\mathrm{y,b}}$ and $f_{\mathrm{u,b}}$ are the material yield and tensile strength of the beam, respectively, $W_{\mathrm{y,b}}$ and $W_{\mathrm{p,b}}$ are the elastic and plastic section moduli of the beam, respectively, b_{c} and t_{fc} are the width and thickness of the column flange, respectively, $M_{\mathrm{p,fc}} = b_{\mathrm{c}}t_{\mathrm{fc}}^2f_{\mathrm{y,cf}}/4$ and $M_{\mathrm{p,st}} = b_{\mathrm{c}}t_{\mathrm{st}}^2f_{\mathrm{y,st}}/4$ are plastic moment resistances of the column flange and the pair of continuity plates, respectively, where t_{st} and $f_{y,st}$ are the thickness and material yield strength of the continuity plates, respectively, α_{pz} is a coefficient taken as 0.95 for one-sided connections by Chinese Standard [35], β is another coefficient, also called transformation parameter in Eurocode 3 [45], to account for the effect of column shears and it should be determined based on the internal force equilibrium. Panel zone strength ratios of the left-hand side to the right-hand side of all the above design equations based on the measured material strength are summarized in Table 5. It is apparent that the weakest panel zone is designed using Chinese Standard, while the strongest using Eurocode 8, as already demonstrated by a previous comparative study [19]. Both the AISC Seismic Provisions and Eurocode 8 rated panel strength lie in the range given by the FEMA bounds. All the specimens satisfied Chinese Standard (ratios larger than 1), but only Specimen B355-C690-PZ8*b* was not qualified with enough panel strength according to AISC Seismic Provisions or Eurocode 8 (ratios less than 1). However, it was this specimen that demonstrated the best plastic rotation and energy dissipation capacities. This indicates that the criteria governing the minimum strength of the panel zone may be relaxed in the AISC code and Eurocodes.

Table 5. Comparison of panel zone strength ratios by Eqs. (5–8)

Specimen label	Chinese Standard	AISC Seismic Provisions	FEMA		Eurocode 8
			Lower bound	Upper bound	
B355-C690-PZ12*a* B355-C690-PZ12*b*	1.64	1.28	1.36	0.91	1.17
B355-C690-PZ10*a* B355-C690-PZ10*b*	1.40	1.11	1.16	0.77	1.01
B355-C690-PZ8*b*	1.02	0.83	0.85	0.56	0.75

5 Conclusions

An experimental study on the cyclic behavior of dual-steel beam-to-column welded flange-bolted web connections, i.e., whose columns and beams were made of Q690 and Q355 grade steels, respectively, was undertaken in this paper. The experimental program consisting of five one-sided connection specimens was intended to investigate the influence of beam-to-column flange welded connection details and panel zone strength. The following conclusions are drawn:

1) All the specimens with intermediate and strong panel zones exhibited weld fracture, as expected, at the beam-to-column flange connections, and this weld fracture was largely affected by the welded connection detail used. The specimen with a weak panel zone exhibited shear fracture of the panel zone.
2) The strong-panel specimens as traditionally welded with backing bars, developed about 15% larger maximum moment resistances than the beam yielding moment, close to the beam full plastic moment; they sustained plastic rotations of 0.01–0.03 rad and cumulative plastic rotations of more than 10 times larger than the yielding rotation.
3) The strong-panel specimens with traditional backing bars, but further reinforced with fillet welds underneath the bottom flange, developed 30% larger maximum moment resistances than the beam yielding moment, or nearly 15% larger than the beam full plastic moment; they sustained plastic rotations of at least 0.03 rad and cumulative plastic rotations of about 50 times larger than the yielding rotation.
4) The weak-panel specimen with the fillet-reinforced backing bar underneath the bottom flange exhibited significant strain hardening in the panel zone by developing a 30% larger maximum moment resistance than the yielding moment of the panel zone. This specimen was able to achieve a maximum plastic rotation of 0.05 rad and a cumulative plastic rotation of over 80% larger than the yielding rotation. Panel zone yielding did not produce adverse effect on the plastic rotation capacity.
5) The welded connection detail with backing bars and reinforced by a fillet weld only underneath the bottom beam flange is adequate for highly ductile seismic demand with a maximum plastic rotation of 0.03rad, while the traditional one with unreinforced backing bars is not. The high-strength steel panel zone is also very ductile with a maximum plastic rotation capacity of 0.04

rad.

It is inferred from this study that those welded flange-bolted web connections with high-strength steel columns generally exhibit excellent inelastic performance with desirable energy dissipation characteristics, if their bottom backing bars are reinforced by fillet welds, and their continuity plate welds and lateral bracing are adequate. Fracture is expected to occur only after plastic rotations larger (sometimes significantly) than 0.03rad. It must be noted that the experiments in this study used to justify this superior performance were on beams with a depth of only 320mm. Further study on connections of larger size beams, especially those with deeper sections, is needed.

Acknowledgments

The authors would like to acknowledge the financial supports for this work by the National Natural Science Foundation of China (Grant Nos. 51638009, 51978279 and 52108145).

References

[1] J. Raoul, H.-P. Günther, Use and application of high-performance steels for steel structures, International Association for Bridge and Structural Engineering (IABSE), Zürich, Switzerland, 2005.

[2] Y. Fukumoto, New constructional steels and structural stability, Engineering Structures 18 (1996) 786–791.

[3] R. Bjorhovde, Development and use of high performance steel, Journal of Constructional Steel Research 60 (2004) 393–400.

[4] G. Shi, F. Hu, Y. Shi, Recent research advances of high strength steel structures and codification of design specification in China, International Journal of Steel Structures 14 (2014) 873–887.

[5] G. Shi, X. Chen, Research advances in HSS structures at Tsinghua University and codification of the design specification, Steel Construction 11 (2018) 286–293.

[6] H. Ban, G. Shi, A review of research on high-strength steel structures, Proceedings of the Institution of Civil Engineers - Structures and Buildings 171 (2018) 625–641.

[7] H. Ban, G. Shi, Y. Shi, Y. Wang, Research progress on the mechanical property of high strength structural steels, Advanced Materials Research 250-253 (2011) 640–648.

[8] G. Shi, X. Zhu, H. Ban, Material properties and partial factors for resistance of high-strength steels in china, Journal of Constructional Steel Research 121 (2016) 65–79.

[9] F. Hu, G. Shi, Constitutive model for full-range cyclic behavior of high strength steels without yield plateau, Construction and Building Materials 162 (2018) 596–607.

[10] H. Kuwamura, T. Suzuki, Low-cycle fatigue resistance of welded joints of high-strength steel under earthquake loading, in: A. L. Arroyo, R. Blázquez, J. Martí (Eds.), Proceedings of the Tenth World Conference on Earthquake Engineering, Balkema, Rotterdam, Madrid, Spain, 1992, pp. 2851–2856.

[11] D. Dubina, A. Stratan, N. Muntean, F. Dinu, Experimental program for evaluation of moment beam-to-column joints of high strength steel components, in: R. Bjorhovde, F. S. K. Bijlaard, L. F. Geschwindner (Eds.), Proceedings of the Sixth International Workshop on Connections in Steel Structures VI, American Institute of Steel Construction, Chicago, Illinois, USA, 2008, pp. 355–366.

[12] S.-H. Oh, H.-Y. Park, A study to enhance the deformation capacity of beam-to-column connections using high strength steel having high yield ratio, International Journal of Steel Structures 16 (2016) 73–89.

[13] F. Liao, X. Li, W. Wang, Y. Chen, T. Zhou, S. Nie, G. Li, Seismic performance study on q460 high-strength steel welded cruciform beam-column connections, Journal of Constructional Steel Research 198 (2022) 107504.

[14] S.-Y. Kim, K.-J. Shin, S.-H. Lee, H.-D. Lee, Experimental investigation of beam-to-column connection with shn490 steel under cyclic loading, International Journal of Steel Structures 16 (2016) 1299–1307.

[15] Z. Wang, S. Zhang, J. Lu, Experimental study on seismic behavior of hybrid high strength steel frame joints, Industrial Construction 48 (2018) 163–168. (in Chinese).

[16] X. Liu, Y. Wang, Y. Shi, Q. Tan, Experimental study on low-cycle fatigue fracture behavior of high strength steel beam-to-column connection, Journal of Building Structures 39 (2018) 28–36. (in Chinese).

[17] J. Lu, Experimental research on the seismic performance of beam-to-column connections in high strength steel frame, 2015. (in Chinese).

[18] F. Hu, G. Shi, Y. Shi, Experimental study on seismic behavior of high strength steel frames: Global response, Engineering Structures 131 (2017) 163–179.

[19] F. Hu, G. Shi, Experimental study on seismic behavior of high strength steel frames: Local response, Engineering Structures 229 (2021) 111620.

[20] X. Chen, G. Shi, Experimental study on seismic behaviour of cover-plate joints in high strength steel frames, Engineering Structures 191 (2019) 292–310.

[21] X. Chen, G. Shi, Cyclic tests on high strength steel flange-plate beam-to-column joints, Engineering Structures 186 (2019) 564–581.

[22] H. Guo, X. Zhou, W. Li, Y. Liu, D. Yang, Experimental and numerical study on seismic performance of q690 high-strength steel plate reinforced joints, Thin-Walled Structures 161 (2021) 107510.
[23] M. Xu, J. Lu, H. Li, G. Shu, Z. Hou, L. Qin, Experimental research on the aseismic behavior of q690gj high strength steel beam-to-column connections considering reinforced panel zone, Steel Construction 31 (2016) 6–13. (in Chinese).
[24] A. M. Girão Coelho, F. S. K. Bijlaard, H. Kolstein, Experimental behaviour of high-strength steel web shear panels, Engineering Structures 31 (2009) 1543–1555.
[25] S. Jordão, L. Simões da Silva, R. Simões, Design formulation analysis for high strength steel welded beam-to-column joints, Engineering Structures 70 (2014) 63–81.
[26] S. Jordão, L. Simões da Silva, R. Simões, Behavior of high-strength steel welded beam-to-column joints with beams of unequal height, in: R. Bjorhovde, F. S. K. Bijlaard, L. F. Geschwindner (Eds.), Proceedings of the Sixth International Workshop on Connections in Steel Structures VI, American Institute of Steel Construction, Chicago, Illinois, USA, 2008, pp. 343–353.
[27] P. Luo, T. Tanaka, H. Asada, Experimental study on elastic-plastic behavior of high-strength steel beam-to-column panel zone considering under-matching welding effect, Engineering Structures 267 (2022) 114655.
[28] D. Dubina, A. Stratan, C. Vulcu, A. Ciutina, High strength steel in seismic resistant building frames, Steel Construction 7 (2014) 173–177.
[29] Ministry of Housing and Urban-Rural Development of the People's Republic of China (MOHURD), Code for seismic design of buildings (2016 edition). GB 50011-2010, China Building Industry Press, Beijing, China, 2018. (in Chinese).
[30] Ministry of Housing and Urban-Rural Development of the People's Republic of China (MOHURD), Technical specification for high strength bolt connections of steel structures. JGJ 82-2011, China Building Industry Press, Beijing, China, 2011. (in Chinese).
[31] SAC Joint Venture, State of the Art Report on Connection Performance, FEMA-355D, Federal Emergency Management Agency, Washington, D.C., USA, 2000.
[32] American Institute of Steel Construction (AISC), Prequalified Connections for Special and Intermediate Steel Moment Frames for Seismic Applications, including Supplements No.1 and No. 2. ANSI/AISC 358-16, ANSI/AISC 358s1-18, ANSI/AISC 358s2-20, American Institute of Steel Construction, Chicago, Illinois, USA, 2020.
[33] Ministry of Housing and Urban-Rural Development of the People's Republic of China (MOHURD), Technical specification for steel structure of tall building. JGJ 99-2015, China Building Industry Press, Beijing, China,

2015. (in Chinese).
[34] Ministry of Housing and Urban-Rural Development of the People's Republic of China (MOHURD), Standard for design of high strength steel structures. JGJ/T 483-2020, China Building Industry Press, Beijing, China, 2020. (in Chinese).
[35] Ministry of Housing and Urban-Rural Development of the People's Republic of China (MOHURD), Standard for design of steel structures. GB 50017-2017, China Building Industry Press, Beijing, China, 2016. (in Chinese).
[36] Standardization Administration of China (SAC), Metallic materials–Tensile testing–Part 1: Method of test at room temperature. GB/T 228.1-2021, Standards Press of China, Beijing, China, 2021. (in Chinese).
[37] American Institute of Steel Construction (AISC), Seismic Provisions for Structural Steel Buildings. ANSI/AISC 341-16, American Institute of Steel Construction, Chicago, Illinois, USA, 2016.
[38] H. Krawinkler, A. Gupta, R. Medina, N. Luco, Loading histories for seismic performance testing of SMRF components and assemblies, Report No. SAC/BD-00/10, SAC Joint Venture, Richmond, California, USA, 2000.
[39] Applied Technology Council (ATC), Guidelines for cyclic seismic testing of components of steel structures. ATC-24, Applied Technology Council, Redwood City, California, USA, 1992.
[40] M. Nakashima, K. Suita, K. Morisako, Y. Maruoka, Tests of welded beam-column subassemblies. I: Global behavior, ASCE Journal of Structural Engineering 124 (1998) 1236–1244.
[41] M. Nakashima, K. Saburi, B. Tsuji, Energy input and dissipation behaviour of structures with hysteretic dampers, Earthquake Engineering and Structural Dynamics 25 (1996) 483–496.
[42] D. Lee, S. C. Cotton, J. F. Hajjar, R. J. Dexter, Y. Ye, Cyclic behavior of steel moment-resisting connections reinforced by alternative column stiffener details. I: Connection performance and continuity plate detailing, AISC Engineering Journal 42 (2005) 189–213.
[43] M. Reynolds, C.-M. Uang, Economical weld details and design for continuity and doubler plates in steel special moment frames, ASCE Journal of Structural Engineering 148 (2022) 04021246.
[44] European Committee for Standardization (CEN), Eurocode 8: Design of structures for earthquake resistance - Part 1: General rules, seismic actions and rules for buildings. EN 1998-1:2004, British Standards Institution (BSI), London, UK, 2004.
[45] European Committee for Standardization (CEN), Eurocode 3: Design of steel structures - Part 1-8: Design of joints. EN 1993-1-8:2005, British Standards Institution (BSI), London, UK, 2005.